A Taylor expansion approach for computing structural performance variation from population-based shape data*

Xilu Wang, **Xiaoping Qian**†
Computational Design & Manufacturing Laboratory
Department of Mechanical Engineering
University of Wisconsin-Madison
Madison, Wisconsin 53705
Email: qian@engr.wisc.edu

Rapid advancement of sensor technologies and computing power has led to wide availability of massive population-based shape data. In this paper, we present a Taylor expansion based method for computing structural performance variation over its shape population. The proposed method takes four steps: 1) learning the shape parameters and their probabilistic distributions through the statistical shape modeling; 2) deriving analytical sensitivity of structural performance over shape parameter; 3) approximating the explicit function relationship between the FE solution and the shape parameters through Taylor expansion; 4) computing the performance variation by the explicit function relationship.

To overcome the potential inaccuracy of Taylor expansion for highly nonlinear problems, a multi-point Taylor expansion technique is proposed, where the parameter space is partitioned into different regions and multiple Taylor expansions are locally conducted. It works especially well when combined with the dimensional reduction of the principal component analysis in the statistical shape modeling.

Numerical studies illustrates the accuracy and efficiency of this method.

Keywords: shape learning, statistical shape modeling, finite element analysis

1 INTRODUCTION

Rapid advancement of sensor miniaturization and growing sensor network and computer power have lead to wide availability of massive shape data from populations of objects. Such massive shape data range from human body shapes in Civilian American and European Surface Anthropometry Resource [1] and Size China [2], to longitudinal knee observations of a large population of osteoarthritis patients [3]. Populations of shape data also include shapes of man-made objects, such as shapes of same manufactured parts due to manufacturing process variation as well as part shapes due to shape degradation after deployment. Mining and analysis of such massive population-based shape data can result in knowledge of shape variability of the population and lead to construction of faithful subject-specific 3D shape models from sparse measurements. It is then possible to predict shape-specific functional performance and population-wide structural performance variation. Such an ability brings about unprecedented capabilities and tantalizing opportunities for mass customization, part-specific failure prediction and just-in-time part maintenance, and patient-specific biomedical intervention and treatment [4,5]. The goal of this work is thus to develop an efficient computer method that can predict 1) shape-specific structural performance from given discrete shape data, and 2) structural performance variation over the shape population.

Our approach builds on statistical analysis of shape variations, a.k.a. statistcal shape modeling (SSM). SSM has emerged as a powerful tool [6] for shape learning from a population where statistical analysis of shape variation is conducted, typically through principal component analysis. It has found its success in various fields including image segmentation [7], motion tracking [8], and parametric shape design [9, 10]. The use of statistical shape modeling techniques to understand shape variations and its effect on biomechanical performance has been recently attempted in [4,11,12,12–14]. However, the computing of the structure performance variation over a population is usually through the Monte Carlo simulation, i.e. by randomly generating the shape parameters according to the learned probabilistic distributions, and obtaining a set of new shapes and new finite element meshes usually through mesh deformation. The finite element analysis is then performed on each of the generated finite element models and the results are collected from which the structural performance variation is obtained. For example, in [14], the performance of the cementless osseointegrated tibial tray in a general population was studied using

*An earlier version of this paper appeared in IDETC 2016
†Corresponding author.

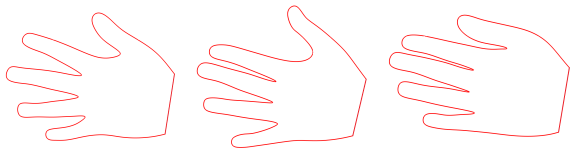

(a) A shape population

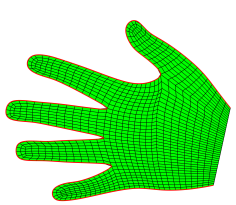

(b) FE mesh of the mean shape

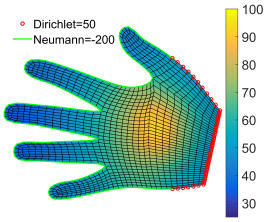

(c) FE result of (b)

(d) Subject-specific temperature distributions from Taylor expansion

Fig. 1. Proposed approach for predicting subject-specific structural performance: Taylor series expansion of the FE solution for the mean shape as applied in a heat transfer problem.

1000 finite element analyses on different subjects. The drawback of such Monte Carlo simulation based approach lies in its inefficiency. In order to obtain a result with reasonable accuracy, a large number of experiments (usually > 500) are needed and each experiment, in this context, requires an expensive finite element analysis.

The advantage of our approach lies in the fact that only one time FE analysis of the mean shape is used to predict the subject-specific shape's structural performance and the performance variation over the population. Figure 1 shows the proposed approach as applied in a heat transfer problem: approximating temperature fields for a shape population with Taylor expansion of the FE solution for the mean shape. Given a population of shapes, the mean shape and the modes of variation are obtained by the statistical shape modeling. A shape instance is then represented as the linear combination of the mean shape and the modes of variation. The weights $\mathbf{w} = [w_1 \cdots w_m]^T$ is called the shape parameters. Based on the shape sensitivity analysis $\partial\mathbf{u}/\partial\mathbf{w}$, where $\mathbf{u}$ is the FE solution, the Taylor expansion is conducted to approximate the function $\mathbf{u}(\mathbf{w})$ and extrapolate the solution on the mean shape to other shapes.

The limitation of usual Taylor expansion lies in its potential inaccuracy for nonlinear problems. In this work, to overcome potential inaccuracy of Taylor expansion, a multi-point based Taylor expansion technique is proposed. The parameter space of the shape population is partitioned into different regions and multiple Taylor expansions are conducted around the local bases within each region. This technique is extremely powerful when combined with the dimensional reduction of principal component analysis (PCA) in SSM. Since as a result of PCA, the first several shape parameters capture a majority of the shape variations. Thus the region partition is only carried with respect to the first few shape parameters and the dimension of the problem has been significantly reduced. To determining the positions of the expansion bases, an optimization based approach is designed.

2 METHOD OVERVIEW

The proposed method involves four steps: 1) statistical shape modeling; 2) shape sensitivity analysis; 3) approximation by Taylor expansion; and 4) computing the performance variation.

The input for our method are the boundary shapes: $\left\{\mathbf{X}_\Gamma^{(k)}, k = 1, \cdots, n_s\right\}$. Firstly, the shape parameters and their probabilistic distributions are learned from the statistical shape modeling. The shapes are parameterized by the eigenshapes $\{\boldsymbol{\psi}_k\}$ and the shape parameters $\{w_k\}$

$$\mathbf{X}_\Gamma = \overline{\mathbf{X}}_\Gamma + \sum_{k=1}^{m} w_k \boldsymbol{\psi}_k,\ w_k \sim N(0, \lambda_k), \tag{1}$$

where $\mathbf{X}_\Gamma$ is the boundary shape, $\overline{\mathbf{X}}_\Gamma$ is mean shape of the population. $w_k \sim N(0,\lambda_k)$ means the kth shape parameter is normally distribution with mean 0 and variance λ_k.

Secondly, the analytical sensitivities of the FE solution $\mathbf{u}$ and the structural performance c with respect to the shape parameters $\mathbf{w} = [w_1, \cdots, w_m]^T$ are calculated

$$\frac{\partial c}{\partial w_k} = \frac{\partial c}{\partial \mathbf{u}^t}\frac{\partial \mathbf{u}}{\partial w_k},\ k = 1, \cdots, m. \tag{2}$$

Then, with the results of sensitivity analysis, an explicit function relationship between the structural performance and the shape parameters is obtained from the Taylor expansion

$$\tilde{c}(\mathbf{w}) = c(\mathbf{0}) + \sum_{k=1}^{m} \frac{\partial c}{\partial w_k} w_k, \tag{3}$$

where $c(\mathbf{0})$ is the structural performance of the mean shape. $\tilde{c}(\mathbf{w})$ is the approximation of $c(\mathbf{w})$.

Finally, the probability distribution $p(\tilde{c})$ of the structural performance is obtained by the explicit function relationship $\tilde{c}(\mathbf{w})$ and the learned probability distribution of the shape parameters $p(\mathbf{w})$.

The output is the cumulative distribution function (CDF) $F_{\tilde{c}}(c^*) = p(\tilde{c} \le c^*)$ of the structural performance $\tilde{c}$, where $p(\tilde{c} \le c^*)$ is the probability that $\tilde{c}$ is less than c^*.

In this study, we use $p(\cdot)$ to denote the probability of a specific event. The boundary shapes are represented by discrete sampling points: $\mathbf{X}_\Gamma = [\mathbf{x}_1, \cdots, \mathbf{x}_{n_b}]^t$, where $\mathbf{x}_i = [x_{i,1}, x_{i,2}]^t$ is vector of coordinates and n_b is the number of sampling points. We use $\mathbf{X}$ to denote the FE mesh in general. When $\mathbf{X}$ appears in the equations, it means the positions of the mesh nodes, for example, $\mathbf{X} = [\mathbf{p}_1, \cdots, \mathbf{p}_{n_p}]^t$, where

$\mathbf{p}_i = [p_{i,1}, p_{i,2}]^t$ is vector of coordinates and n_p is the number of mesh nodes. We use $\mathbf{u}$ to denote the FE solution in general. When $\mathbf{u}$ appears in the equations, it means the nodal values of the FE solution, for example, $\mathbf{u} = [u_1, \cdots, u_{n_p}]^t$. If $\mathbf{u}$ is an $n_p \times 1$ vector and $\mathbf{w}$ is an $m \times 1$ vector, $\frac{\partial \mathbf{u}}{\partial \mathbf{w}^t}$ would be an $n_p \times m$ matrix, its element in the ith row and jth column is $\frac{\partial u_i}{\partial w_j}$.

3 STATISTICAL SHAPE MODELING

Statistical shape modeling plays important roles in computing the structural performance variation over a shape population. It computes the mean shape and the modes of variations in a population. It captures the variability of shapes in space through the probability distribution of the learned shape parameters. The mean shape of the population provides a statistical atlas, based on which we create the template FE mesh. The statistical shape modeling usually contains three steps: shape registration, shape alignment, and shape analysis.

Given a population of shapes $\left\{\mathbf{X}_{raw}^{(1)}, \cdots, \mathbf{X}_{raw}^{(n_s)}\right\}$, they can be registered to a reference shape by the rigid [6] or the non-rigid shape registration techniques [15, 16], or could by cross-parameterization [17]. In this work, the shape registration is conducted by deforming the given shapes to the reference shape through the iterative free-form deformation [16], by which the boundary correspondences between the reference shape and the given shapes are obtained. Then, the shapes are re-sampled by the same number of points in correspondence and are aligned to the same coordinate frame, for example, by generalized Procrustes analysis [18]. These re-sampled shapes are $\mathbf{X}_\Gamma^{(k)} = [\mathbf{x}_1^{(k)}, \cdots, \mathbf{x}_{n_b}^{(k)}]^t$, $k = 1, \cdots, n_s$, where n_s is the number of training shapes, and n_b is the number of sampling points on each shape.

The principal component analysis (PCA) is then conducted for capturing shape variations and dimensional reduction. In PCA, each shape is treated as a vector in $\mathbb{R}^{2n_b}$, the mean shape of the population is

$$\overline{\mathbf{X}}_\Gamma = \frac{1}{n_s} \sum_{k=1}^{n_s} \mathbf{X}_\Gamma^{(k)}, \tag{4}$$

the shape covariance matrix is

$$\mathbf{\Sigma} = \frac{1}{n_s - 1} \mathbf{\Phi}\mathbf{\Phi}^T, \tag{5}$$

where $\mathbf{\Phi} = [\mathbf{X}_\Gamma^{(1)} - \overline{\mathbf{X}}_\Gamma, \cdots, \mathbf{X}_\Gamma^{(n_s)} - \overline{\mathbf{X}}_\Gamma]$. Just as all the covariance matrices do, the shape covariance matrix $\mathbf{\Sigma}$ describes the patterns and ranges of variations from the mean $\overline{\mathbf{X}}_\Gamma$. Through eigen-decomposition, we have

$$\mathbf{\Sigma}\boldsymbol{\psi}_k = \lambda_k \boldsymbol{\psi}_k, \; k = 1, \cdots, n_s - 1, \tag{6}$$

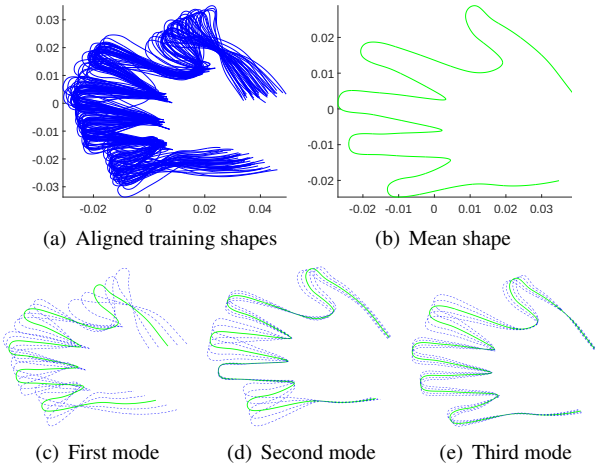

(a) Aligned training shapes (b) Mean shape

(c) First mode (d) Second mode (e) Third mode

Fig. 2. Statistical shape modeling of hand shapes: (a) 40 aligned training shapes; (b) the mean shape: $\overline{\mathbf{X}}_\Gamma$; (c) the first mode by varying w_1: $\overline{\mathbf{X}}_\Gamma + w_1\boldsymbol{\psi}_1$; (d) the second mode by varying w_2: $\overline{\mathbf{X}}_\Gamma + w_2\boldsymbol{\psi}_2$; (e) the third mode by varying w_3: $\overline{\mathbf{X}}_\Gamma + w_3\boldsymbol{\psi}_3$.

where $\boldsymbol{\psi}_1, \cdots, \boldsymbol{\psi}_{n_s-1}$ are the principal components of $\mathbf{\Sigma}$, $\lambda_1, \cdots, \lambda_{n_s-1}$ are the corresponding eigenvalues. The principal components captures the modes of shape variations. The eigenvalues are the amount of variances in those components.

Through PCA, the shapes are modeled as the linear combination of the mean shape and the variation modes

$$\mathbf{X}_\Gamma = \overline{\mathbf{X}}_\Gamma + \sum_{k=1}^{m} w_k \boldsymbol{\psi}_k, \tag{7}$$

where $\mathbf{X}_\Gamma$ is a shape modeled by PCA, $\boldsymbol{\psi}_k, k = 1, \cdots, m$ are the first m variation modes. The number of modes, m, can be determined, e.g. from $\sum_{k=1}^{m} \lambda_k / \sum_{k=1}^{n_s-1} \lambda_k \geq 98\%$, which means that the first m modes should capture more than 98% of the total shape variances in the training set. $w_k, k = 1, \cdots, m$ are the corresponding weights. We call them the shape parameters and note $\mathbf{w} = [w_1, \cdots, w_m]^t$.

In Figure 2 we show an example of statistical shape modeling of 40 hand shapes, from which we see the mean shape of the population and the first three modes of shape variations. As a result of dimensionality reduction, the first three shape modes captures 66.6%, 16.6%, and 7.8% of the total shape variances respectively.

The shape parameters $\{w_k\}$ are assumed to be normally distributed. They are uncorrelated with each other as the result of PCA. The probabilistic distribution of the shapes in $\mathbb{R}^{2n_b}$ is then modeled by the distributions of the first m shape parameters as

$$w_k \sim N(0, \sigma_k), \; k = 1, \cdots, m,$$

where $N(0, \sigma_k)$ stands for the normal distribution with 0 mean and standard deviation $\sigma_k = \sqrt{\lambda_k}$.

4 SHAPE SENSITIVITY ANALYSIS

Through statistical shape modeling, a shape in the population is parameterized by the shape parameters $\mathbf{w}$. In this section we derive the analytical sensitivity of the FE solution $\mathbf{u}$ over the shape parameters $\mathbf{w}$. Assume we have the FE state equation

$$\mathbf{K}(\mathbf{w})\mathbf{u} = \mathbf{b}(\mathbf{w}), \tag{8}$$

the sensitivity of the FE solution over the shape parameters is calculated by [19]

$$\frac{\partial \mathbf{u}}{\partial w_k} = \mathbf{K}^{-1}\left(\frac{\partial \boldsymbol{b}}{\partial w_k} - \frac{\partial \mathbf{K}}{\partial w_k}\mathbf{u}\right), k = 1, \cdots, m. \tag{9}$$

For a specific element e in the stiffness matrix $\mathbf{K}$ or the loading vector $\mathbf{b}$, by the chain rule we have

$$\frac{\partial e}{\partial w_k} = \frac{\partial e}{\partial \mathbf{X}^t}\frac{\partial \mathbf{X}}{\partial \mathbf{X}_\Gamma^t}\frac{\partial \mathbf{X}_\Gamma}{\partial w_k}, \tag{10}$$

where $\frac{\partial e}{\partial \mathbf{X}^t}|_{1\times 2n_p}$ is the sensitivity of element e with respect to the mesh nodes, it is calculated according to the governing equations of the finite element method [19–21]; $\frac{\partial \mathbf{X}}{\partial \mathbf{X}_\Gamma^t}|_{2n_p\times 2n_b}$ is the sensitivity of the mesh nodes with respect to the boundary points, it is calculated based on the Thin-plate deformation, whose details will be given later; and $\frac{\partial \mathbf{X}_\Gamma}{\partial w_k}|_{2n_b\times 1}$ is the sensitivity of the boundary points with respect to the shape parameters and from equation (7) we have

$$\frac{\partial \mathbf{X}_\Gamma}{\partial w_k} = \boldsymbol{\psi}_k,\ k = 1, \cdots, m. \tag{11}$$

The only unknown in equation (10) now is $\frac{\partial \mathbf{X}}{\partial \mathbf{X}_\Gamma^t}$. Here the thin-plate deformation (TPS) [22] is used to transfer the boundary perturbations to the interior nodes due to its simplicity and robustness. It is worth mentioning that other deformation methods could also be applied, for example, the free-form deformation [23], the deformation by pseudo linear elasticity [24].

The formulation of the thin-plate deformation is

$$\boldsymbol{\Phi}(\mathbf{x}) = \mathbf{c} + \mathbf{A}\mathbf{x} + \mathbf{V}^t\mathbf{U}(\mathbf{x}), \tag{12}$$

where $\mathbf{x} = [x_1, x_2]^t$ is the domain point and is deformed to $\boldsymbol{\Phi}(\mathbf{x})$; $\mathbf{c} = [c_1, c_2]^t$ is the translation vector; $\mathbf{A}$ is the 2×2 affine transformation matrix; $\mathbf{V}^t\mathbf{U}(\mathbf{x})$ is the deformation part, where $\mathbf{U}(\mathbf{x}) = [\rho(\mathbf{x}-\overline{\mathbf{x}}_1^\Gamma), \cdots, \rho(\mathbf{x}-\overline{\mathbf{x}}_{n_b}^\Gamma)]^t$ is the $n_b \times 1$ vector of kernel functions, $\overline{\mathbf{x}}_1^\Gamma, \cdots, \overline{\mathbf{x}}_{n_b}^\Gamma$ are the coordinates of boundary points with $\overline{\mathbf{x}}_i^\Gamma = [\overline{x}_{i,1}^\Gamma, \overline{x}_{i,2}^\Gamma]^t$, and $\mathbf{V} = [\mathbf{v}_1, \cdots, \mathbf{v}_{n_b}]^t$ is the $n_b \times 2$ matrix of TPS weights with $\mathbf{v}_i = [v_{i,1}, v_{i,2}]^t$. The kernel function ρ is defined as

$$\rho(h) = \begin{cases} \|h\|^2 \log(\|h\|), & \|h\| > 0; \\ 0, & \|h\| = 0. \end{cases} \tag{13}$$

Given the coordinates of the initial boundary points $\overline{\mathbf{x}}_1^\Gamma, \cdots, \overline{\mathbf{x}}_{n_b}^\Gamma$, and the coordinates of the perturbed boundary points $\mathbf{x}_1^\Gamma, \cdots, \mathbf{x}_{n_b}^\Gamma$, the translation vector $\mathbf{c}$, affine transformation matrix $\mathbf{A}$ and the deformation weights $\mathbf{V}$ can be solved as [6, 22]:

$$\mathbf{V} = \mathbf{B}^{11}\mathbf{X}_\Gamma,\ \begin{bmatrix} \mathbf{c}^t \\ \mathbf{A}^t \end{bmatrix} = \mathbf{B}^{21}\mathbf{X}_\Gamma, \tag{14}$$

where $\overline{\mathbf{X}}_\Gamma = [\overline{\mathbf{x}}_1^\Gamma, \cdots, \overline{\mathbf{x}}_{n_b}^\Gamma]^t$ is the $n_b \times 2$ matrix of initial boundary points, $\mathbf{X}_\Gamma = [\mathbf{x}_1^\Gamma, \cdots, \mathbf{x}_{n_b}^\Gamma]^t$ is the $n_b \times 2$ matrix of perturbed boundary points. In this paper the mean shape $\overline{\mathbf{X}}_\Gamma$ is set as the initial boundary. $\mathbf{B}^{11}$ $(n_b \times n_b)$ and $\mathbf{B}^{21}$ $(3 \times n_b)$ are coefficient matrices decided by the positions of the initial boundary points $\overline{\mathbf{X}}_\Gamma$, whose closed form formulation is given in [6].

Substituting (14) into (12), we have

$$\boldsymbol{\Phi}(\mathbf{x}) = \mathbf{X}_\Gamma^t\mathbf{B}^{12}\begin{bmatrix} 1 \\ \mathbf{x} \end{bmatrix} + \mathbf{X}_\Gamma^t\mathbf{B}^{11}\mathbf{U}(\mathbf{x}), \tag{15}$$

where $\mathbf{B}^{12}$ is the transpose of $\mathbf{B}^{21}$.

Assume $\overline{\mathbf{X}} = [\overline{\mathbf{p}}_1, \cdots, \overline{\mathbf{p}}_{n_p}]^t$ the nodes of the FE mesh of the mean shape $\overline{\mathbf{X}}_\Gamma$, and $\mathbf{X} = [\mathbf{p}_1, \cdots, \mathbf{p}_{n_p}]^t$ the nodes of the deformed FE mesh. We have $\mathbf{X}$ as a linear function of the boundary points $\mathbf{X}_\Gamma$

$$\mathbf{X} = \left([\mathbf{1}, \overline{\mathbf{X}}^t]\mathbf{B}^{21} + \mathbf{U}^t(\overline{\mathbf{X}})\mathbf{B}^{11}\right)\mathbf{X}_\Gamma, \tag{16}$$

where $\mathbf{U}(\overline{\mathbf{X}}) = [\mathbf{U}(\overline{\mathbf{p}}_1), \cdots, \mathbf{U}(\overline{\mathbf{p}}_{n_p})]$. From equation (16) we have the sensitivity of the mesh nodes with respect to the boundary points

$$\frac{\partial \mathbf{X}}{\partial \mathbf{X}_\Gamma^t} = \begin{pmatrix} [\mathbf{1}, \overline{\mathbf{X}}^t]\mathbf{B}^{21} + \mathbf{U}^t(\overline{\mathbf{X}})\mathbf{B}^{11} & \\ & [\mathbf{1}, \overline{\mathbf{X}}^t]\mathbf{B}^{21} + \mathbf{U}^t(\overline{\mathbf{X}})\mathbf{B}^{11} \end{pmatrix}, \tag{17}$$

on the left side of the equation $\mathbf{X}$ and $\mathbf{X}_\Gamma$ are vectorized.

Now, we have the sensitivity of the FE nodal solutions $\frac{\partial \mathbf{u}}{\mathbf{w}^t}$ from equations (9) and (10). The sensitivity of the structural performance $\frac{\partial c}{\partial \mathbf{w}^t}$ can be easily obtained by the chain rule:

$$\frac{\partial c}{\partial \mathbf{w}^t} = \frac{\partial c}{\partial \mathbf{u}^t}\frac{\partial \mathbf{u}}{\partial \mathbf{w}^t}. \tag{18}$$

5 TAYLOR APPROXIMATION OF STRUCTURAL PERFORMANCE

The Taylor expansion is used to explicitly approximate the function relationship $c(\mathbf{w})$ between the structural performance c and the shape parameters $\mathbf{w}$.

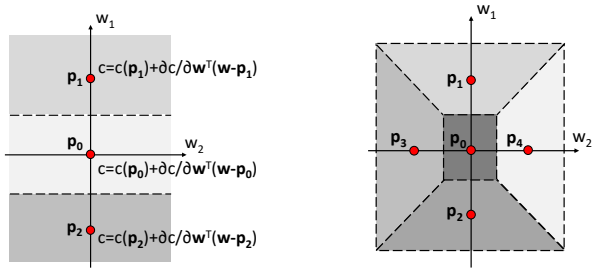

(a) Three regions (b) Five regions

Fig. 3. Partition the domain into different regions and conduct Taylor expansion in each region separately.

5.1 Single point Taylor expansion

In the single point Taylor expansion, the performance function $c(\mathbf{w})$ is expanded around the mean shape, where the shape parameters are zeros.

$$\tilde{c}(\mathbf{w}) = c(\mathbf{0}) + \frac{\partial c}{\partial \mathbf{w}^t}\mathbf{w}, \tag{19}$$

where $c(\mathbf{0}) = c(\mathbf{u}(\mathbf{0}))$, and $\mathbf{u}(\mathbf{0})$ is the FE solution on the mean shape solved from the below equation:

$$\mathbf{K}(\mathbf{0})\mathbf{u} = \mathbf{b}(\mathbf{0}). \tag{20}$$

5.2 Multi-point Taylor expansion

To overcome the potential inaccuracy of Taylor expansion at points far away from the mean shape, a multi-point Taylor expansion technique is proposed.

As shown in Figure 3 are two different examples of the multi-point Taylor expansion. In Figure 3(a) the domain has been partitioned into three regions by the two dashed horizontal lines. The Taylor expansions are conducted locally in each region around the bases $\mathbf{p}_i, i = 0,1,2$. In Figure 3(b) the domain has been partitioned into five regions. The procedure of the multi-region Taylor expansion is as follows:

1. Choosing n number of expansion bases $\{\mathbf{p}_0, \mathbf{p}_1, \cdots, \mathbf{p}_n\}$.
2. Partition the parametric domain into n regions $\Omega_0, \Omega_1, \cdots, \Omega_n$ according to the closest distance to the base points:

$$\Omega_i = \left\{ \mathbf{w} \mid \|\mathbf{w} - \mathbf{p}_i\| = \min_{j=0,\cdots,n} \|\mathbf{w} - \mathbf{p}_j\| \right\}.$$

3. Approximate $c(\mathbf{w})$ piece-wisely by the Taylor expansions around the local bases:

$$\tilde{c}(\mathbf{w}) = \begin{cases} c(\mathbf{p}_0) + \frac{\partial c}{\partial \mathbf{w}^T}(\mathbf{w} - \mathbf{p}_0), \ \forall \mathbf{w} \in \Omega_0 \\ \vdots \\ c(\mathbf{p}_n) + \frac{\partial c}{\partial \mathbf{w}^T}(\mathbf{w} - \mathbf{p}_n), \ \forall \mathbf{w} \in \Omega_n \end{cases} \tag{21}$$

It should be noted that, though $\tilde{c}(\mathbf{w})$ may not be continuous, the obtained probability distribution $p(\tilde{c})$ will be close to that of the true performance $p(c)$ as long as $\tilde{c}(\mathbf{w})$ is close to $c(\mathbf{w})$.

Choosing appropriate expansion bases $\mathbf{p}_0 \cdots \mathbf{p}_n$ is critical in the multi-point Taylor expansion. For each point $\mathbf{w}$, it is expanded with respect to the closest base point. So the range of extrapolation at $\mathbf{w}$ is $l(\mathbf{w}) = \min_{j=0,\cdots,n} \|\mathbf{w} - \mathbf{p}_j\|$. Since the error of Taylor expansion is propositional to $l(\mathbf{w})^{r+1}$, where r is the degree of expansion and in this paper $r = 1$, it is desirable to minimize the overall squared range of extrapolation. However, each shape parameter $\mathbf{w}$ does not appear in the same frequency, the accuracy of approximation is more important at the regions of high probability. Based on that, an objective function is designed:

$$\min_{\{\mathbf{p}_j\}} \ E = \int_{\Omega} l(\mathbf{w})^2 p(\mathbf{w}) d\mathbf{w}, \tag{22}$$

where the extrapolation range $l(\mathbf{w})^2$ is weighted by the probability density $p(\mathbf{w})$ and is integrated over the whole domain. Note that $l(\mathbf{w})$ in equation (22) is a minimum formula and will cause obstacles for the optimization. Since the p-norm is widely used in approximating the minimum and maximum formulas, $l^2(\mathbf{w}) = \min_{j=0,\cdots,n} \|\mathbf{w} - \mathbf{p}_j\|^2$ is substituted by $(\sum_{i=0}^{n} l_j^{-2q})^{-\frac{1}{q}}$. Considered that the probability density $p(\mathbf{w})$ of the shape parameters is original symmetric as in equation (24), it is desirable to have the expansion bases symmetric with respect to the origin. At last, we have the optimization formula:

$$\begin{aligned} \min_{\{\mathbf{p}_j\}} \ & E = \int_{\Omega} (\sum_{i=0}^{n} l_j^{-2q})^{-\frac{1}{q}} p(\mathbf{w}) d\mathbf{w}, \\ \text{s.t.} \ & \mathbf{p}_j = -\mathbf{p}_{n-j}, j = 0, \cdots, n. \end{aligned} \tag{23}$$

Locations of expansion bases are then obtained from (23) through a gradient decent approach.

6 Probabilistic distribution of the structural performance

Through the Taylor expansion, an explicit function relationship $\tilde{c}(\mathbf{w})$ between the shape parameters $\mathbf{w}$ and the structural performance c is obtained. By the statistical shape modeling, the probability density function of the shape parameters are learned:

$$p(\mathbf{w}) = \Pi_{k=1}^{m} (2\pi\lambda_k)^{-\frac{1}{2}} e^{-\frac{w_k^2}{2\lambda_k}}, \tag{24}$$

where w_k is the kth shape parameter and λ_k is the shape variance in the kth principal direction.

The cumulative distribution function of the approximated structural performance $\tilde{c}$ is given by:

$$F_{\tilde{c}}(c^*) = p(\tilde{c} \leq c^*) = \int_{\tilde{c}(\mathbf{w}) \leq c^*} p(\mathbf{w}) d\mathbf{w}. \quad (25)$$

6.1 Closed form solution

If the obtained structural performance $\tilde{c}$ is linear and continuous as in equation (19), since it is assumed that the shape parameters are normally distributed, we have that $\tilde{c}$ is also normally distributed with mean $c(\mathbf{0})$ and variance:

$$\lambda_c = \frac{\partial c}{\partial \mathbf{w}^t} \Lambda \frac{\partial c}{\partial \mathbf{w}}, \quad (26)$$

where $\Lambda = \text{diag}(\lambda_1 \cdots \lambda_m)$ is the covariance matrix of $\mathbf{w}$. The closed form of equation (25) is then obtained accordingly.

6.2 Monte Carlo integration

If the obtained structural performance $\tilde{c}$ is discontinuous as in equation (21). A closed form of equation (25) is either non-existent or very hard to obtain. In such cases, the Monte Carlo integration [25] is used to integrate the cumulative probability function (25). Compared with the finite element analysis, the function evaluations of $\tilde{c}(\mathbf{w})$ by (21) cost nothing.

7 NUMERICAL RESULTS

In this section, the influence of geometrical variation on the structural performances have been studied with a 2D heat transfer problem and a 2D elasticity problem. We examine the numerical accuracy of the Taylor expansion for various modes of shape variations. We also compare the distributions of the structural performances obtained by Taylor expansion with those obtained by the Monte Carlo simulation.

The evaluation process of Monte Carlo simulation (MCS) is as follows:

1. Randomly generate $N \geq 500$ sets of shape parameters $\{\mathbf{w}_i\}$ according to $p(\mathbf{w})$.
2. For each shape parameter $\mathbf{w}_i$, generate the corresponding boundary shape $\mathbf{X}_\Gamma^{(i)}$ by the statistical shape model (7).
3. Generate the finite element mesh $\mathbf{X}^{(i)}$ for $\mathbf{X}_\Gamma^{(i)}$ by the thin-plate deformation of the FE mesh of the mean shape (16).
4. Conduct the FE analysis, record the results and repeat steps 2,3,4 until $i = N$.

In our numerical study, the 40 hand shapes in [26] are used as the training set as in Figure 2. Each shape is represented by $n_b = 2001$ number of discrete points. We model the shape variations among them through the statistical shape modeling method as detailed in [16]. The first 8 shape modes is used to compactly represent the overall shape variation,

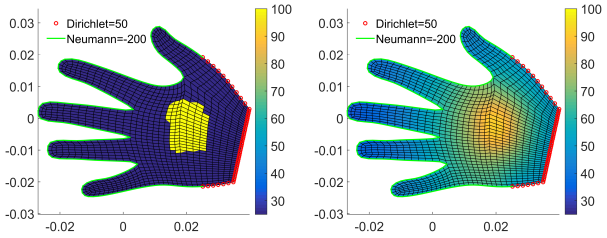

(a) Boundary conditions on the mean shape (b) FE solution

Fig. 4. A 2D heat transfer problem: Dirichlet boundary condition $u = 50$ on Γ_1 (red circle), Neumann boundary condition $\frac{\partial u}{\partial \mathbf{n}} = -200$(green boundary), thermal load: $q = 1000000$ in the center of the hand (yellow area).

which captures more than 98% of the total shape variance. The template FE mesh is created on the mean shape and has $n_p = 1250$ number of nodes.

7.1 2D heat transfer problem

The 2D heat transfer is governed by the Poisson equation:

$$-\Delta u = q \text{ in } \Omega \quad (27)$$

$$u = T_1 \text{ on } \Gamma_1 \quad (28)$$

$$\frac{\partial u}{\partial \overrightarrow{n}} = g \text{ on } \Gamma_2 \quad (29)$$

where u is the temperature, q is the thermal load, Ω is the domain of heat transfer, Γ_1 is the Dirichlet boundary, T_1 is the boundary temperature, Γ_2 is the Neumann boundary, and g is the Neumann boundary condition.

Figure 4 shows the 2D heat transfer on the hand shape. Figure 4(a) shows the FE mesh of the mean shape and the boundary conditions. Figure 4(b) shows the corresponding FE solution. In this example, the variability of the thermal compliance $c = \int_\Omega qud\Omega$ due to the shape variations is studied.

7.1.1 Temperature distribution by Taylor expansion

Figure 5 shows the predicted temperature distribution of shapes due to the change of the first shape parameter. We can see that as w_1 increases from $-2\sigma_1$ to $2\sigma_1$ in Figure 5(a), 5(b), 5(c), and 5(d), the hand becomes more expanded, and the temperature in the field decreases.

In order to examine the accuracy of Taylor expansion, here we compare the results predicted by the Taylor expansion with the ones obtained by the finite element analysis.

The Taylor expansion of the nodal temperatures $\mathbf{u}(\mathbf{w})$ and the thermal compliance $c(\mathbf{w})$ around the mean are done through equation (19). The finite element analysis are conducted at the designed points, as shown by the stars $*$ in Figure 7. At each point, a new shape is generated by the corresponding shape parameters, the FE mesh is obtained by the thin-plate deformation of the FE mesh of the mean shape and a new FE analysis is conducted.

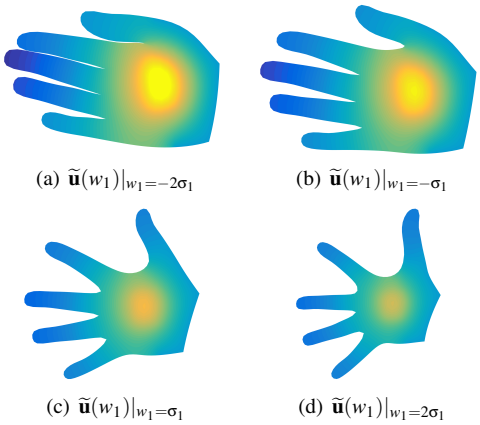

(a) $\widetilde{\mathbf{u}}(w_1)|_{w_1=-2\sigma_1}$ (b) $\widetilde{\mathbf{u}}(w_1)|_{w_1=-\sigma_1}$

(c) $\widetilde{\mathbf{u}}(w_1)|_{w_1=\sigma_1}$ (d) $\widetilde{\mathbf{u}}(w_1)|_{w_1=2\sigma_1}$

Fig. 5. Predicted temperature distribution due to shape variations in the first mode. The color means the temperature, and its range follows the same color bar as in Figure 4.

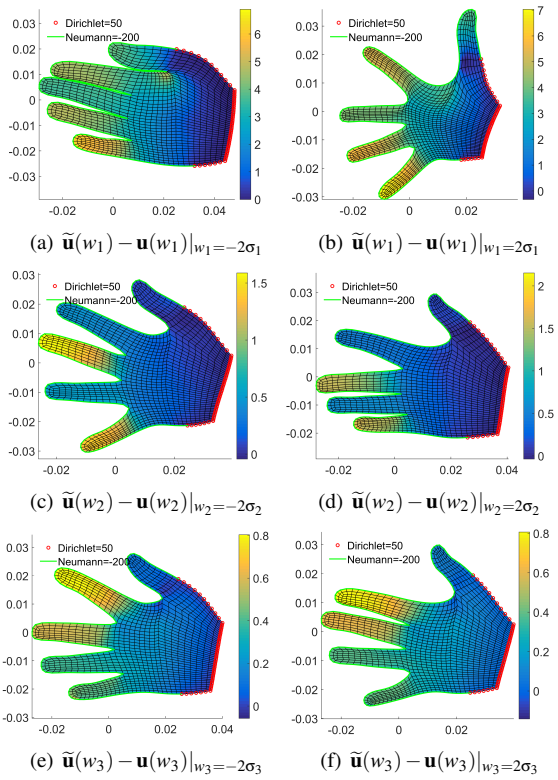

(a) $\widetilde{\mathbf{u}}(w_1)-\mathbf{u}(w_1)|_{w_1=-2\sigma_1}$ (b) $\widetilde{\mathbf{u}}(w_1)-\mathbf{u}(w_1)|_{w_1=2\sigma_1}$

(c) $\widetilde{\mathbf{u}}(w_2)-\mathbf{u}(w_2)|_{w_2=-2\sigma_2}$ (d) $\widetilde{\mathbf{u}}(w_2)-\mathbf{u}(w_2)|_{w_2=2\sigma_2}$

(e) $\widetilde{\mathbf{u}}(w_3)-\mathbf{u}(w_3)|_{w_3=-2\sigma_3}$ (f) $\widetilde{\mathbf{u}}(w_3)-\mathbf{u}(w_3)|_{w_3=2\sigma_3}$

Fig. 6. The errors between the temperatures predicted by Taylor expansion and from FE analysis.

Figure 6(a) and 6(b) show the errors between the temperatures predicted by Taylor expansion and from FE analysis with shape change in the first mode. The results are obtained by varying the first shape parameter from negative two standard deviations to positive two standard deviations, while keeping all the other shape parameters 0. The maximum errors in Figure 6(a) and 6(b) are 6.89 and 7.03, respectively, while the scale of temperature variation in our FE solution is about 80 as shown in Figure 4. We could see that the maximum error happens at the tip of the little finger, where the shape variation is large and is far from the Dirichlet boundary. The Taylor expansion extrapolates the FE solution of the mean shape to other shapes, so it is reasonable to expect that the maximum error happens at the farthest extrapolation point (large shape deviation). Since the temperature on the Dirichlet boundary is fixed, so there is no error on the Dirichlet boundary.

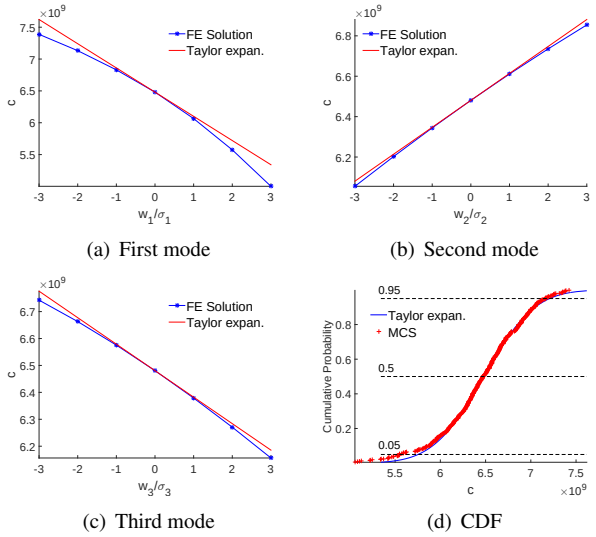

(a) First mode (b) Second mode

(c) Third mode (d) CDF

Fig. 7. Comparing Taylor expansion with FE analysis of thermal compliance: (a) $\widetilde{c}=c(0)+w_1\partial c/\partial w_1$; (b) $\widetilde{c}=c(0)+w_2\partial c/\partial w_2$; (c) $\widetilde{c}=c(0)+w_3\partial c/\partial w_3$; (d) cumulative distribution functions from Taylor expansions and from 500 Monte Carlo simulations.

Figure 6(c) and 6(d) compare the Taylor expansion with the FE solutions for shape changes along the second mode. The maximum errors in Figure 6(c) and 6(d) are 1.59 and 2.15, respectively. Figure 6(e) and 6(f) compares the Taylor expansion with the FE solutions for shape changes along the third mode. The maximum errors in Figure 6(e) and 6(f) are 0.80 and 0.81, respectively.

It could be seen that from the first mode to the third mode, the errors become smaller and smaller. That's because as a result of PCA, the first mode captures a majority of the total shape variances and the remaining modes captures fewer and fewer shape variances. So the deviation from the mean shape becomes smaller and smaller.

7.1.2 Thermal compliance by Taylor expansion

Figure 7(a) shows the relationship between the first shape parameter w_1 and the thermal compliance c by Taylor expansion and from the FE analysis. Since the thermal load q as in Figure 4(a) is added in the middle area, where has small extrapolation errors as in Figure 7(a), the results of Taylor expansion $\tilde{c}$ is close to the FE analysis c. The maximum relative error (max $|\widetilde{c}-c|/c$) is 6.77%.

Figure 7(b) and 7(c) show the relationships between the second and third shape parameters with the thermal compliance. The results of Taylor expansion agree well with the finite element analysis, the maximum relative errors are 0.42% and 0.49% respectively.

Since the Taylor expansions in Figure 7(a), 7(b), and

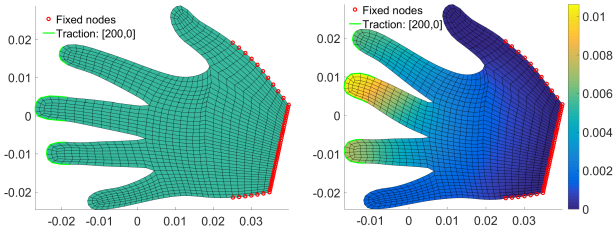

(a) Boundary conditions on the mean shape (b) Nodal displacements

Fig. 8. A 2D linear elasticity problem: (a) FE model of the mean shape: Dirichlet boundary condition $\hat{\mathbf{u}} = [0,0]^T$ on Γ_D (red circle), Neumann boundary condition $\hat{\mathbf{t}} = [200,0]^T$ (green boundary); (b) the resulting nodal displacements, the color shows the values of horizontal displacements.

7(c) gives relatively small extrapolation errors, the single-point Taylor expansion (19) around the mean shape is used to approximate $c(\mathbf{w})$ and calculate the cumulative probability function (CDF) of the thermal compliance. In this case we have the analytical solution (26). The result is shown in Figure 7(d), it can be seen that the analytical CDF conforms well to that obtained by the Monte Carlo simulations. The three horizontal curves in Figure 7(d) partition the space into four intervals at the cumulative probabilities of 5%, 50%, and 95%. From the two inner intervals we could see that, for about 90% of the shapes in the population, the thermal compliance c should be within the range $[5.8\times10^9, 7.1\times10^9]$. The run time for the Taylor expansion based approach is 2.88s including the sensitivity calculation. The run time for the 500 Monte Carlo simulations is 106.54s. The computing is performed with MATLAB on the processor of "intel(R) Core(TM) i7-5500U".

7.2 2D elasticity problem

The governing PDEs of the linear elasticity problem are

$$-\nabla\cdot\boldsymbol{\sigma} = \mathbf{f} \text{ in } \Omega, \tag{30}$$

$$\boldsymbol{\sigma} = 2\mu\boldsymbol{\varepsilon} + \lambda(\nabla\cdot\mathbf{u})\mathbf{I} \text{ in } \Omega, \tag{31}$$

$$\boldsymbol{\varepsilon} = \frac{1}{2}(\nabla\mathbf{u} + \nabla\mathbf{u}^T) \text{ in } \Omega, \tag{32}$$

$$\mathbf{u} = \hat{\mathbf{u}} \text{ on } \Gamma_D, \tag{33}$$

$$\boldsymbol{\sigma}\mathbf{n} = \hat{\mathbf{t}} \text{ on } \Gamma_N, \tag{34}$$

where $\boldsymbol{\sigma}$ is the domain stress, $\mathbf{f}$ is the domain force, Ω is the domain, $\mathbf{u}$ is the displacement, $\mathbf{I}$ is the identity matrix, $\hat{\mathbf{u}}$ is the fixed displacement on the Dirichlet boundary Γ_D, and $\hat{\mathbf{t}}$ is the traction on the Neumann boundary Γ_N.

In this example, the variability of the structural compliance $c = \int_{\Gamma_N}\mathbf{u}^T\hat{\mathbf{t}}d\Gamma$ due to the shape variations is studied.

Figure 8(a) shows the FE model $\overline{\mathbf{X}}$ of the mean shape $\overline{\mathbf{X}}_\Gamma$ and the boundary conditions. Figure 8(b) shows the solved nodal displacements.

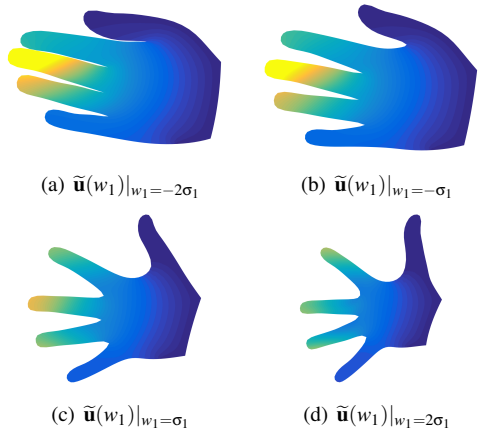

(a) $\tilde{\mathbf{u}}(w_1)|_{w_1=-2\sigma_1}$ (b) $\tilde{\mathbf{u}}(w_1)|_{w_1=-\sigma_1}$

(c) $\tilde{\mathbf{u}}(w_1)|_{w_1=\sigma_1}$ (d) $\tilde{\mathbf{u}}(w_1)|_{w_1=2\sigma_1}$

Fig. 9. Taylor expansion predicted nodal displacements due to shape variations in the first mode. The color shows the values of horizontal displacements and its range follows the same color bar as in Figure 11.

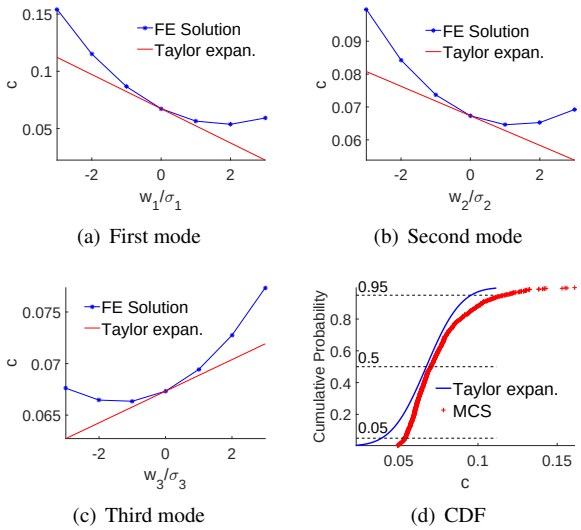

(a) First mode (b) Second mode

(c) Third mode (d) CDF

Fig. 10. Comparing Taylor approximation with FE solutions of structural compliance.

7.2.1 Nodal displacements by Taylor expansion

In this section we display the nodal displacements predicted from the Taylor expansion of equation (19) for shapes with varying shape parameters.

Figure 9 shows the predicted nodal displacements of shapes due to the change of the first shape parameter. As w_1 increases from $-2\sigma_1$ to 2σ in Figure 9(a), 9(b), 9(c), and 9(d), the hand becomes more expanded and smaller, and the displacements decreases.

7.2.2 Structural compliance by Taylor expansion

In this section the single-point Taylor expansion around the mean shape (19) is used to obtain the cumulative distribution function of the structural compliance.

Figure 10(a),10(b), and 10(c) plot the relationship between the first, second, and third shape parameters and the resulting structural compliance c by the Taylor expansions

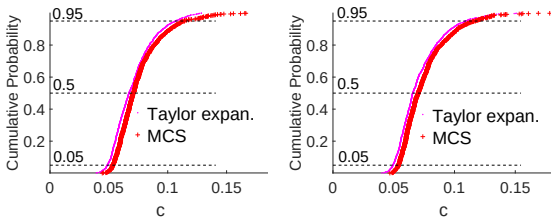

(a) Three bases (b) Five bases

Fig. 11. Cumulative distribution function by multi-point Taylor expansion: (a) result with three expansion bases; (b) result with five expansion bases.

and from the FE analysis. It could be seen that the results of Taylor expansion deviates a lot from that of the FE analysis.

Figure 10(d) compares the cumulative distribution function of the structural compliance $\widetilde{c}$ obtained by the Taylor expansion with the one obtained by 500 Monte Carlo simulations. We can see that the analytical CDF obtained by the Taylor expansion deviates a lot from the CDF obtained by the Monte Carlo simulations.

7.2.3 Multi-point Taylor expansion

The drawback of Taylor expansion lies in the fact that the approximation error becomes larger as the range of extrapolation increases. For certain problems, for example the 2D elasticity problem in this paper, it will cause large discrepancy between the approximated function $\tilde{c}(\mathbf{w})$ and the real one $c(\mathbf{w})$, and thus large discrepancy between the corresponding cumulative distribution functions. By observing Figure 10(a), 10(b) and 10(c), it can be seen that the response of the real FE analysis is quit curved and the Taylor expansion of the points far away from the mean shape deviates a lot from the real FE solution. To overcome this issue, the multi-point Taylor expansion technique, as discussed in section 5.2, is used.

Figure 11 shows the results obtained by the multi-point Taylor expansion. We can see that the cumulative distribution function obtained by the Multi-point Taylor expansion conform well with that of the Monte Carlo simulation. The expansion bases $\{\mathbf{P}_0 \cdots \mathbf{P}_n\}$ are obtained by the optimization formula (22). In this example, the multi-point Taylor expansion is only carried with respect to the first three shape parameters (w_1, w_2, w_3), which captures 91.0% of the total shape variances $\sum_{i=1}^{3} \sigma_i^2 / \sum_{i=1}^{40} \sigma_i^2 = 0.91$.

With $n = 2$, the obtained expansion bases are: $(1.107, 0, 0)$, $(0, 0, 0)$, $(-1.107, 0, 0)$, the result is shown in Figure 11(a). With $n = 4$, the obtained expansion bases are: $(1.764, 0, 0)$, $(-0.798, 0, 0)$, $(0, 0, 0)$, $(0.798, 0, 0)$, $(-1.764, 0, 0)$, the result is shown in Figure 11(b). It is very interesting to notice that all the expansion bases are arranged along the first dimension. This perhaps can be ascribed to the fact that the 1st mode captures 66.7% of the total shape variances.

The run time for the multi-point Taylor expansion is 12.98s with $n = 2$ and 21.86s with $n = 4$ including the sensitivity calculation. The run time for the 500 Monte Carlo simulations is 133.86s. The computing is performed with MATLAB on the processor of "intel(R) Core(TM) i7-5500U".

8 Conclusion

In this paper, we have presented a Taylor expansion based method for efficiently computing structural performance variation over a shape population. Each shape in the population is represented as discrete points. These shapes are then aligned together by generalized Procrustes analysis. Principal component analysis is conducted to obtain the shape variation, which is represented as a sum of variations in multiple principal modes. Finite element analysis is conducted on the mean shape. For each shape specified by the shape parameters, we then invoke a thin-plate deformation based scheme to automatically deform the mesh nodes. The performance of the shapes is approximated via Taylor expansion of the FE solution of the mean shape.

Our Taylor expansion approach allows efficient computing of structural performance variations over a shape population without conducting a large number of FE analysis. The technical contributions of this work include: 1) We have derived the analytical sensitivity of the FE solution with respect to the shape parameters and applied it in the Taylor series approximation of the FE solutions. Numerical results confirms its accuracy with respect to FE solutions. 2) We have demonstrated that the multi-point Taylor expansion technique can effectively overcomes the potential inaccuracy of Taylor expansion when combined with the dimensionality reduction of principal component analysis.

Future work includes extending the current approach to 3-dimensional problems. Our Taylor expansion is linear and the use of multi-point Taylor expansion makes it possible to account for non-linearity. For shapes with large variations, it would be interesting to compare our multi-point Taylor expansion with higher-order approximations.

In this work, shape parameters are assumed to be normally distributed. For shape sets where the shape parameters are not normally distributed, especially when involving pose changes [27], alternative techniques [28] can be considered.

References

[1] Robinette, K. M., Blackwell, S., Daanen, H., Boehmer, M., and Fleming, S., 2002. Civilian american and european surface anthropometry resource (caesar), final report. volume 1. summary. Tech. rep., DTIC Document.

[2] Ball, R., and Molenbroek, J., 2008. "Measuring chinese heads and faces". In Proceedings of the 9th international congress of physiological anthropology. Human diversity: design for life, pp. 150–5.

[3] OAI, 2017. The osteoarthritis initiative (OAI). `https://oai.epi-ucsf.org/datarelease/About.asp`. [Online; 2017-01-25].

[4] Bryan, R., Nair, P. B., and Taylor, M., 2009. "Use of a statistical model of the whole femur in a large scale,

multi-model study of femoral neck fracture risk". *Journal of Biomechanics,* ***42***(13), pp. 2171–2176.

[5] Bischoff, J. E., Dai, Y., Goodlett, C., Davis, B., and Bandi, M., 2014. "Incorporating population-level variability in orthopedic biomechanical analysis: A review". *Journal of Biomechanical Engineering,* ***136***(2), p. 021004.

[6] Dryden, I. L., and Mardia, K. V., 1998. *Statistical Shape Analysis*, Vol. 4. J. Wiley Chichester.

[7] Heimann, T., and Meinzer, H.-P., 2009. "Statistical shape models for 3D medical image segmentation: a review". *Medical Image Analysis,* ***13***(4), pp. 543–563.

[8] Cremers, D., 2006. "Dynamical statistical shape priors for level set-based tracking". *Pattern Analysis and Machine Intelligence, IEEE Transactions on,* ***28***(8), pp. 1262–1273.

[9] Baek, S.-Y., and Lee, K., 2012. "Parametric human body shape modeling framework for human-centered product design". *Computer-Aided Design,* ***44***(1), pp. 56–67.

[10] Chu, C.-H., Tsai, Y.-T., Wang, C. C., and Kwok, T.-H., 2010. "Exemplar-based statistical model for semantic parametric design of human body". *Computers in Industry,* ***61***(6), pp. 541–549.

[11] Bryan, R., Mohan, P. S., Hopkins, A., Galloway, F., Taylor, M., and Nair, P. B., 2010. "Statistical modelling of the whole human femur incorporating geometric and material properties". *Medical Engineering & Physics,* ***32***(1), pp. 57–65.

[12] Galloway, F., Worsley, P., Stokes, M., Nair, P., and Taylor, M., 2012. "Development of a statistical model of knee kinetics for applications in pre-clinical testing". *Journal of Biomechanics,* ***45***(1), pp. 191–195.

[13] Rao, C., Fitzpatrick, C. K., Rullkoetter, P. J., Maletsky, L. P., Kim, R. H., and Laz, P. J., 2013. "A statistical finite element model of the knee accounting for shape and alignment variability". *Medical Engineering & Physics,* ***35***(10), pp. 1450–1456.

[14] Galloway, F., Kahnt, M., Ramm, H., Worsley, P., Zachow, S., Nair, P., and Taylor, M., 2013. "A large scale finite element study of a cementless osseointegrated tibial tray". *Journal of Biomechanics,* ***46***(11), pp. 1900–1906.

[15] Chui, H., and Rangarajan, A., 2003. "A new point matching algorithm for non-rigid registration". *Computer Vision and Image Understanding,* ***89***(2), pp. 114–141.

[16] Wang, X., and Qian, X., 2016. "A statistical atlas based approach to automated subject-specific FE modeling". *Computer-Aided Design,* ***70***, pp. 67–77.

[17] KwoK, T.-H., Zhang, Y., and Wang, C. C., 2012. "Efficient optimization of common base domains for cross parameterization". *IEEE Transactions on Visualization and Computer Graphics,* ***18***(10), pp. 1678–1692.

[18] Gower, J. C., 1975. "Generalized procrustes analysis". *Psychometrika,* ***40***(1), pp. 33–51.

[19] Reh, S., Beley, J.-D., Mukherjee, S., and Khor, E. H., 2006. "Probabilistic finite element analysis using ansys". *Structural Safety,* ***28***(1), pp. 17–43.

[20] Choi, K. K., and Kim, N.-H., 2006. *Structural sensitivity analysis and optimization 1: linear systems*. Springer Science & Business Media.

[21] Qian, X., 2010. "Full analytical sensitivities in NURBS based isogeometric shape optimization". *Computer Methods in Applied Mechanics and Engineering,* ***199***(29), pp. 2059–2071.

[22] Bookstein, F. L., 1989. "Principal warps: Thin-plate splines and the decomposition of deformations". *IEEE Transactions on Pattern Analysis & Machine Intelligence*(6), pp. 567–585.

[23] Sederberg, T. W., and Parry, S. R., 1986. "Free-form deformation of solid geometric models". *ACM SIGGRAPH Computer Graphics,* ***20***(4), pp. 151–160.

[24] Wang, X., and Qian, X., 2014. "An optimization approach for constructing trivariate B-spline solids". *Computer-Aided Design,* ***46***, pp. 179–191.

[25] Hammersley, J. M., 1960. "Monte carlo methods for solving multivariable problems". *Annals of the New York Academy of Sciences,* ***86***(3), pp. 844–874.

[26] Stegmann, M. B., and Gomez, D. D., 2002. "A brief introduction to statistical shape analysis". *Informatics and Mathematical Modelling, Technical University of Denmark, DTU,* ***15***, p. 11.

[27] Hasler, N., Stoll, C., Sunkel, M., Rosenhahn, B., and Seidel, H.-P., 2009. "A statistical model of human pose and body shape". In Computer Graphics Forum, Vol. 28, Wiley Online Library, pp. 337–346.

[28] Chen, X., Zheng, C., and Zhou, K., 2016. "Example-based subspace stress analysis for interactive shape design". *IEEE Transactions on Visualization and Computer Graphics*.